International Journal of Nanomedicine

Dovepress
open access to scientific and medical research

Open Access Full Text Article

ORIGINAL RESEARCH

Peptide-Based HDL as an Effective Delivery System for Lipophilic Drugs to Restrain Atherosclerosis Development

Junwei Gao[1], Ziyun Li[1], Jing Li[2], Ping Song[3], Jinsheng Yang[1], Wei Xiao[4], Ning Li[1], Ruodan Xu[1]

[1]Department of Biomedical Engineering and Technology, Institute of Basic Theory for Chinese Medicine, China Academy of Chinese Medical Sciences, Beijing, People's Republic of China; [2]Department of Nephropathy, Dongzhimen Hospital, Beijing University of Chinese Medicine, Beijing, People's Republic of China; [3]Department of Dermatology, Guang'anmen Hospital, China Academy of Chinese Medical Sciences, Beijing, People's Republic of China; [4]Key Laboratory of New-Tech for Chinese Medicine Pharmaceutical Process, Jiangsu Kanion Pharmaceutical Co. Ltd., Lianyungang, People's Republic of China

Correspondence: Ruodan Xu; Ning Li, Email ruodanxu@gmail.com; lili.li.ning@gmail.com

Purpose: Peptide-based high-density lipoprotein (pHDL) structurally and functionally resembles the natural HDL as anti-atherosclerosis (AS) therapies. Since pHDL contains a large hydrophobic core, this study aims to evaluate the potentials of pHDL as a hydrophobic drug carrier and the efficiency of drug-loaded pHDL in the control of AS.

Methods: The pHDL encapsulation of hydrophobic components from natural plants, including curcumin (Cur) and tanshinone IIA (TanIIA), was achieved using one-step microfluidics. Then, morphological features and loading efficiencies of pHDL-Cur and pHDL-TanIIA were determined by TEM and high-performance liquid chromatography (HPLC), respectively. Taking the fluorescence advantage of Cur, localizations of loaded Cur in pHDL were investigated by fluorescence quenchers, and recruitments of Cur to AS plaques were assessed with ex vivo imaging. Based on anti-inflammatory properties of TanIIA, pHDL-TanIIA was accordingly developed to evaluate the anti-AS effects through examinations of plasma lipid parameters and pathological alterations of plaque-associated regions.

Results: Both lipophilic Cur and TanIIA can be efficiently loaded into pHDL carriers. The resultant pHDL-Cur and pHDL-TanIIA inherit the homogeneous nano-disk structure of pHDL. By using pHDL-Cur, the encapsulated hydrophobics are tracked in the core of pHDL, and incorporations of Cur with pHDL vehicles greatly improve the bioavailability and association of Cur with AS plaques. Moreover, when loaded with TanIIA, which has established its role in anti-AS as an anti-inflammatory candidate, synergistic effects in reducing AS lesions and improving pathological alterations of main organs related to AS were achieved.

Conclusion: The pHDL system could potentially be applied for both imaging and therapy in animal models of AS. Benefits of pHDL-based drug delivery will potentially extend the application scenarios of bioactive chemicals from natural plants which are underutilized due to features like low bioavailability and facilitate the clinical translation of synthetic HDL therapies in HDL-associated disorders, including but not limited to AS.

Keywords: HDL, peptide-based HDL, atherosclerosis, drug delivery, natural plants, antiatherogenic therapy

Introduction

Cardiovascular disease (CVD) remains the global leading cause of mortality, taking 17.9 million lives in 2019 corresponding to 32% of overall deaths according to the World Health Organization (WHO) estimates (https://www.who.int/en/news-room/fact-sheets/detail/cardiovascular-diseases-(cvds)). CVD is usually caused by atherosclerosis (AS), the pathophysiological behaviors of which are associated with lipid-driven inflammatory responses of the arterial intima.[1–4] Although lipid-lowering medications, such as statins, are the most prescribed drugs for clinical management of AS, side effects like liver injury, renal insufficiency and muscle pain have been reported.[5] Given the equal importance of inflammation in AS, anti-inflammatory therapies, with interleukin-1 receptor antagonist (IL-1Ra) and the blocker of IL-6 receptor (IL-6Rb) being the most promising approaches, are entering clinics for AS-associated conditions. However, a long-term systemic application of IL-1Ra and IL-6Rb is limited by unfavorable side effects in metabolism.[6,7] With the frequent occurrence of unwanted adverse effects in current interventions for

Received: 17 May 2022
Accepted: 8 August 2022
Published: 6 September 2022

Graphical Abstract

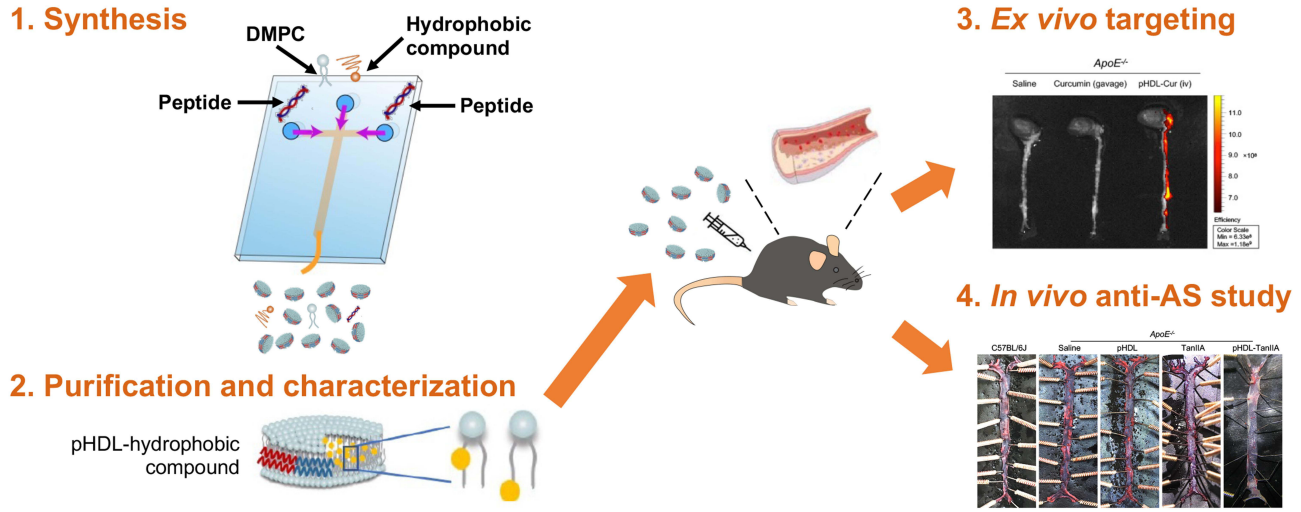

AS, efforts have been shed light on the use of drug delivery system to improve the pharmacological properties of anti-AS drugs, and more importantly to potentially extend the application scenarios of bioactive chemicals from natural plants which are underutilized due to features like low bioavailability.

The integration of nanotechnology into drug delivery systems has been extensively studied.[8] With the rapid nanotechnological advances made in cancer, multifunctional nanocarriers based on liposomes, micelles, inorganic, and polymeric nanoparticles have also been engineered for the development of AS therapies.[9] Of note, synthetic high-density lipoprotein (HDL) nanoparticles, which mimic the structure and/or function of native HDL, have attracted increasing attention in the diagnosis and drug delivery for a wide range of disorders, especially for AS.[10,11] Mechanistically, being the "good cholesterol", biofunctions of HDL are mainly reflected by reverse cholesterol transport (RCT) through a direct interaction between the major HDL component apolipoprotein A-I (ApoA-I) and the receptors associated with atherosclerotic plaques, such as ATP-binding cassette transporters A1 (ABCA1) and G1 (ABCG1) and possibly the scavenger receptor B1 (SR-B1).[12] Moreover, being surrounded by apolipoproteins and phospholipids, HDL nanoparticles contain a large hydrophobic core of cholesteryl ester and triglycerides, which enables a high loading capacity for lipophilic molecules.[13] Altogether, these inherent features render HDL mimetic nanoparticles "the nature's drug delivery system" for AS therapeutics.

Based on the natural architecture and compositions of HDL, a series of attempts have been exerted to optimize the manufacture of HDL nanoparticles. Conventionally, HDL is isolated and obtained from human blood plasma by sequential density ultracentrifugation (SD-UC) or fast protein liquid chromatography (FPLC).[14] However, the apparently low concentration of resultant HDL and the potential immunogenicity of plasma dramatically limit the purification of large amounts of HDL and its application into pivotal clinical development. Additionally, a diversity of methods have been developed to artificially synthesize HDL mimetics, such as lipid film dispersion, sodium cholate dialysis, thermal cycling, high-pressure homogenization, and microfluidics.[15–20] Among the above techniques, the utilization of microfluidics has been shown to facilitate the production of synthetic nanoparticles into more reproducible and homogeneous formulations, in which the size and morphology of HDL particles can be fine-tuned by manipulating the mixing composition, ratio, and speed in continuous flow conditions. The other concern raised by the regular approaches in HDL reconstitution is the involvement of ApoA-I because the large size and the complexity in the synthesis and purification of full-length ApoA-I proteins have set great financial and manufacturing barriers to the HDL-based drug delivery. To tackle these challenges, our group has recently succeeded in developing peptide-based HDL (pHDL) simply using microfluidics with 1,2-dimyristoyl-sn-glycero-3-phosphocholine (DMPC) and the mimetic peptide derived from ApoA-I as starting materials. We demonstrate that the combination of microfluidics and mimetic peptides offers a more

affordable, feasible and controllable approach to produce mimetic HDL. Meanwhile, the produced pHDL nanoparticles share similar physicochemical and biological properties with native HDL in the prevention of AS development.[21]

Considering that the features of pHDL core are suitable for incorporating hydrophobic drugs, in the current study, we desire to investigate the potential of pHDL in the encapsulation of lipophilic ingredients from natural plants, including the tanshinone IIA (TanIIA) isolated from natural plant Danshen (Salvia miltiorrhiza Bunge) and curcumin from Curcuma longa.[22–25] Then, to validate the feasibility and affordability of pHDL drug delivery system in the context of AS, the plaque-targeting and anti-AS capacities of drug-loaded pHDL were further evaluated according to the specific nature of TanIIA and curcumin.

Materials and Methods

Materials

DMPC was purchased from Avanti Polar Lipids, Inc. (Alabaster, AL, USA). The C-terminal amidated 4F dimer peptides, which contains 37 amino acids, with one proline provided in between two 4F sequences, were synthesized by GenScript Inc. (Nan Jing, Jiang Su, China). The purity of the peptides was determined to be over 95% by reverse HPLC. TanIIA (>98% purification) was purchased from Yuanye Biotechnology Co., Ltd (Shanghai, China), and curcumin (>98% purification) was purchased from Ronghe Pharmaceutical Technology Development Co., Ltd (Shanghai, China). All reagents used in HPLC were purchased from Fisher Scientific (Fair Lawn, NJ, USA).

Synthesis of pHDL-TanIIA and pHDL-Cur Nanoparticles

The construction of drug-loaded pHDL using the microfluidic device was modified according to our established protocols for the synthesis of pHDL nanoparticles, as described in detail previously.[21] Briefly, TanIIA- or curcumin-loaded pHDL nanoparticles were prepared by injecting into the middle channel of the microfluidic chip a mixture of DMPC with either TanIIA (50–1500 μg/mL) or curcumin (100–1000 μg/mL) dissolved in ethanol (5 mg/mL) at a rate of 1 mL/min. Solutions of mimetic peptides in ddH_2O (0.2 mg/mL) were injected into two external channels at a rate between 2.5 and 10 mL/min for the optimal strategy. For the purpose of visualizing pHDL localization in vivo, fluorescein isothiocyanate (FITC)-Ahx was added to the N-terminal of mimetic peptides (FITC-pHDL), where indicated. The resultant products were collected from the outlet channel and then washed and concentrated with Amicon® ultra centrifugal filters (10 K MWCO, Millipore, Billerica, MA, USA).

Scanning Electron Microscopy (SEM) Characterization

The morphological features of the TanIIA or curcumin particles were analyzed using SEM, respectively. In brief, the solid samples of TanIIA or curcumin were transferred onto the carbon tape mounted on an SEM stage. Prior to SEM, the samples were coated with gold using ion sputter coater (SBC-12, KYKY Technology Co., Ltd., Beijing, China) for 1 min. Then, the images were obtained using the Phenom SEM (Phenom ProX, Eindhoven, the Netherlands) at 10 KV in high vacuum mode.

Transmission Electron Microscopy (TEM) Characterization

Following the purification of drug-loaded pHDL nanoparticles, the solution was properly diluted with ddH_2O. Then, 10 μL diluted samples were placed onto carbon-coated copper grids (Electron Microscopy Sciences, Hatfield, PA, USA). After 60 seconds, the samples were negatively stained with 10 μL 2% sodium phosphotungstate (Sigma-Aldrich, St. Louis, MO, USA). Once stained and air-dried, the TEM grids can be stored until further TEM observation. Images were taken with a Hitachi H7650 TEM microscope (Tokyo, Japan) at 80 kV. The diameter of nanoparticles was analyzed using Image J (National Institute of Health, Bethesda, Maryland, USA).

Analytical Procedures

The percentage of peptides and encapsulated TanIIA or curcumin was determined by UV absorption spectroscopy (Allsheng Instruments CO., Ltd., Hangzhou, China) and high-performance liquid chromatography (HPLC, Agilent, Palo Alto, USA), respectively. In chromatography, C18 column was used as the stationary phase (Agilent, Stable

Bond 300, 4.6 mm × 250 mm, 5 μm), and the mobile phase was either composed of methanol and H_2O (75:25, v/v) or acetonitrile and H_2O (45:55, v/v) at a flow rate of 1 mL/min with the retention time being 15 min. The amounts of TanIIA and curcumin were quantified at 275 nm and 425 nm, respectively. The encapsulation efficiency and drug loading efficiency of TanIIA or curcumin were calculated according to the following equation:

$$\text{Encapsulation Efficiency}(\%) = \text{Amount of drug in NPs}/\text{Amount of drug initially taken to prepare the NPs} \times 100$$

$$\text{Drug Loading Efficiency}(\%) = \text{Weight of drugin NPs}/\text{Weight of NPs} \times 100$$

Spectroscopic Characterization of Curcumin and pHDL-Cur

The presence of curcumin in pHDL was determined based on its intrinsic absorbance and fluorescence properties. Initially, ultraviolet–visible (UV-Vis) absorbance spectra of curcumin were recorded from 200 to 700 nm (Varioskan, Thermo Scientific, Waltham, MA, USA) in ethanol and compared with that of free curcumin in ddH_2O or pHDL-Cur in ddH_2O. Fluorescence emission spectra of free curcumin in ddH_2O, curcumin in ethanol or pHDL-Cur were measured using a fluorescence spectrophotometer (Varioskan) from 430 to 600 nm (5 nm slit width) at 420 nm excitation.

Quenching Studies

To verify the location of curcumin in pHDL nanoparticles, the fluorescence emission of curcumin was quenched with potassium iodide (KI) and spin-labeled fatty acids (5-DSA and 16-DSA). Briefly, fluorescence quenching by KI was performed by addition of small increments of stock solutions of KI in PBS to pHDL-Cur. Likewise, quenching with 5-DSA or 16-DSA was carried out by addition of stock solutions in DMSO. Fluorescence emission intensities were recorded at 495 nm following excitation at 420 nm. Quenching data were analyzed using the Stern-Volmer equation, $F_0/F = 1 + Ksv(Q)$, where F_0 and F are fluorescence intensities in the absence and presence of varying quencher concentrations, respectively, Q is the quencher concentration, and Ksv is the apparent quenching constants.[26,27]

DPPH Free Radical Scavenging Assay

This assay offers a quantitative approach for evaluating antioxidant capacity of compounds by spectrophotometrically measuring the color decay of the stable free radical 2,2-Diphenyl-1-picrylhydrazyl (DPPH) with the interaction of compounds. DPPH has a characteristic maximum absorption at 517 nm, but upon reduction by an antioxidant, its absorption decreases. Here, the antioxidant activities of free curcumin and pHDL-Cur were examined according to the procedure developed by Blois.[28] While based on the data obtained from encapsulation efficiency of pHDL-Cur, curcumin samples were prepared with the same curcumin concentrations as that in pHDL-Cur. In brief, free curcumin or pHDL-Cur at various concentrations (0.1–30 μg/mL) was added separately at a 1:1 volume ratio to each 0.1 mg/mL DPPH in ethanol solution. After 30 min incubation in the dark at room temperature, the absorbance of each solution was measured at 517 nm against control samples lacking scavenger using the following formula:

$$\text{Scavenging rate}(\%) = \left(\begin{array}{l} 1 - \text{absorbance of test sample with DPPH} - \text{absorbance of test sample without DPPH}/ \\ \text{absorbance of blank with DPPH} \end{array} \right) \times 100$$

Stability Assay of Drug-Loaded pHDL Nanoparticles

The in vitro stability study of drug-loaded pHDL nanoparticles (pHDL-Cur and pHDL-TanIIA) was performed with freshly prepared nanoparticles incubated in either ddH_2O or FBS at 37°C for various periods of 0, 0.17, 0.33, 0.5, 0.67, 1, 2, 6 and 12 h. Samples were then centrifuged and the supernatants were collected to determine the abundance of encapsulated drug kept in pHDL. UV–Vis spectroscopy and HPLC were used to quantify curcumin and TanIIA encapsulated in pHDL, respectively.

Animal Model and Treatment

Five-week-old male apolipoprotein E-deficient (*ApoE*$^{-/-}$, B6.129P2-ApoE$^{tm1Unc/j}$) mice and C57BL/6J mice were purchased from Peking University Laboratory Animal Center (Beijing, China). All experimental animals were group-housed in a controlled environment (23 ± 3°C, 55 ± 15% humidity, 12 h light/dark cycle) with free access to food and water throughout the experimental period. All animal studies were conducted according to the National Guidelines for Care of Laboratory animals and performed in accordance with institutional regulations with approval of experimental protocols by the Institutional Animal Care and Use Committee of the Institute of Basic Theory for Chinese Medicine, China Academy of Chinese Medical Sciences. After 7-day adaptation, C57BL/6J mice were fed a standard chow diet (CD), while *ApoE*$^{-/-}$ mice received a high fat diet (HFD, Beijing Keao Xieli Feed Co. Ltd., Beijing, China), containing 21% (wt/wt) fat and 0.15% cholesterol throughout the duration of the experiments. After 8-week pre-feeding with HFD, 6-week intraperitoneal (ip) injection of pHDL (13 mg/kg calculated by the amount of mimetic peptides, 2 injections per week, N = 7), pHDL-TanIIA (13 mg/kg mimetic peptides, corresponding to 11 mg/kg TanIIA, 2 injections per week, N = 7), or saline placebo (2 injections per week, N = 7), as well as oral administration of TanIIA suspension in saline (30 mg/kg per day, N = 6) were conducted. The body weight of mice was regularly monitored each week, and at the end of the experimental period, the blood and tissues of experimental animals were collected for further analyses.

Biodistribution

Dynamic profiles of circulating pHDL-Cur were measured using 9-month-old male *ApoE*$^{-/-}$ mice challenged with either curcumin suspended in 0.5% carboxymethyl cellulose at a dose of 200 mg/kg by gavage or pHDL-Cur (13 mg/kg mimetic peptides, corresponding to 2.5 mg/kg curcumin) through *ip*, with saline administered by *ip* as control. 0, 0.3, 0.5, 1, 2, 3, 4, 8 h post drug exposure, blood samples of each group were collected, and the abundance of pHDL-Cur was determined by quantification of curcumin in blood using fluorescence spectrophotometry. Biodistribution of pHDL-Cur in different tissues was determined using tissues collected at 0.5 h post pHDL-Cur exposure by *ip*. Basically, 500 μL RIPA buffer (Solarbio) containing 1% protease inhibitor cocktail was added to 50 mg tissues, followed by homogenization at 70 Hz for 120 s and centrifugation at 18,705 × g, 4°C for 10 min.

Ex vivo and in vivo Fluorescence Imaging

To characterize the ability of pHDL in plaque-targeted delivery of entrapped drugs, ex vivo imaging was carried out using IVIS® Lumina II Imaging System (Caliper Life Sciences, Waltham, MA, USA). Male *ApoE*$^{-/-}$ mice of 9-month on HFD were randomly divided into three groups, with those challenged with pHDL-Cur (corresponding to 14 mg/kg curcumin) or saline by intravenous (iv) injections via the lateral tail veins, while mice treated with curcumin suspended 0.5% carboxymethyl cellulose (200 mg/kg) through gavage. Thirty minutes after drug exposure, the hearts and aortas were quickly isolated and imaged with excitation at 430 nm and emission at 530 nm, which were established and tested to reflect the fluorescent imaging of curcumin. Since the recruitment of pHDL itself to the regions of plaque in vivo has been confirmed previously by immunohistochemistry,[21] we additionally assessed the plaque-localizing effects of pHDL at the level of entire tissue and whole animals using FITC-pHDL.

Blood Tests

All mice were fasted overnight before the collection of blood samples using EDTA-containing tubes. Blood samples were centrifuged at 998 × g, 4°C for 15 min twice, and then analyzed for biochemical parameters, including total cholesterol (TC), serum triglyceride (TG), low-density lipoprotein cholesterol (LDL-C), alanine aminotransferase (ALT), aspartate aminotransferase (AST), globulin, and blood creatinine using biochemical analyzer (Olympus Japan Co., Ltd., Japan).

Histochemistry

At the end of the experiments, the relevant tissues of experimental mice were fixed in 10% phosphate buffered formalin solution, embedded in paraffin, and then sectioned into 4-μm-thick slices (6 μm for heart) using a microtome (Leica, Nussloch, Germany). The tissues from paraffin-embedded sections were dried in a 45°C constant temperature box for 1

h, deparaffinized in Histo-Clear (National Diagnostics Co., Atlanta, GA, USA) twice at room temperature and then re-hydrated. For hematoxylin eosin (H&E) staining, the re-hydrated tissues were stained in Cole's hematoxylin solution (Solarbio, Beijing, China), according to manufacturer's protocol. For Masson trichrome staining, the re-hydrated tissues were stained with Masson trichrome staining kit (Solarbio), based on manufacturer's guide. For en face Oil Red O (Sigma) staining of the whole aorta, the aorta is dissected out from the heart until 3–5 mm after the iliac bifurcation. After removing the outside fat and connective tissues, the aorta was opened longitudinally and stained with Oil Red O for 15 min. Then, Oil Red O was clean with 70% ethanol, which was further rinsed by running water before image capture. All images were taken using an optical microscope (Nikon ECLIPSE CI-S, Nikon, Tokyo, Japan) with an image analysis system (Nikon DS-U3).

Immunohistochemistry (IHC)

Tissue slides for immunochemistry staining were prepared as described above. For CD68 IHC staining, sections were pre-treated using heat-mediated antigen retrieval with SignalStain Citrate Unmasking Solution (Cell Signaling Technology, USA), followed by washing with Dulbecco's Phosphate Buffered Saline (DPBS, Solarbio). Blocking of endogenous peroxidases was carried out with treatment in a solution of 30% methanol, 3% H_2O_2 in PBS for 30 min, and blocking of nonspecific binding was performed by incubation in PBS supplemented with 5% goat serum, 1% BSA and 0.3% Triton 100X (Sigma-Aldrich). Sections were then incubated with rabbit anti-CD68 antibody (1:100, Abcam, Cambridge, MA, USA) at 4°C overnight. The enhanced goat anti-rabbit biotinylated secondary antibody (ZSGB-BIO, Beijing, China) was used to detect the primary antibody and visualized using an HRP conjugated ABC system (ZSGB-BIO). DAB was used as the chromogen. Sections were then counterstained with hematoxylin, dehydrated through ethanol, cleaned in Histo-Clear, and mounted with neutral balsam. All images were taken using an optical microscope (Nikon ECLIPSE CI-S) with an image analysis system (Nikon DS-U3).

Statistical Analysis

All data are presented as mean value ± the standard error of the mean (SEM) and were analyzed with the one-way analysis of variance (ANOVA) with Bonferroni pairwise corrections and the Student's *t*-test. Values are considered to be significant at a *P* value less than 0.05. We determined that a sample size of 7 mice/group would provide a power of ≥90% with a two-sided type I error of 5% to detect a 20% reduction in the areas of plaque lesions. All statistical analysis was performed, and figures were created using Prism 9 (GraphPad, San Diego, CA, USA).

Results and Discussion

Currently, the application of nanotechnology for drug delivery in AS has been illuminated as an accessible approach for bioactive compounds with low bioavailability. However, due to the uncertainty in biocompatibility of nanomaterials, the translation of such systems into clinically effective nanomedicines remains challenging.[29] Previous studies from our group have shown that the native HDL mimics pHDL, which is constituted by DMPC phospholipids and amphipathic peptides derived from ApoA-I, reserving the activities of HDL in counteracting the development of AS without detectable signs of unfavorable toxicity.[21] Specifically, the unique architecture of pHDL, showing a domed discoidal shape of phospholipid bilayers with a hydrophobic core wrapping by amphipathic molecules, endows pHDL with potential loading capability for lipophilic drugs. In order to further define pHDL as a carrier for hydrophobic compounds, we selected TanIIA and curcumin, two lipophilic extracts from natural plants that were believed to have versatile pharmacological activities on CVD,[30,31] and then attentively characterized the associated features including water solubility, loading pattern and efficiency, rate of biological clearance, and plaque-recruiting potentials when either TanIIA or curcumin was encapsulated in pHDL.

Synthesis and Characterization of Drug-Loaded pHDL Nanoparticles

When preparing nano-drugs, due to the insolubility of TanIIA and curcumin in water, we separately dissolved these compounds with DMPC in ethanol as the solution to be injected into the central channel of microfluidic chip, while keeping solutions of mimetic peptides to be injected via bilateral channels. A direct success of pHDL-Cur preparation was achieved when the same

Table 1 Encapsulation and Loading Efficiency of Curcumin into pHDL

Concentration of Curcumin (μg/mL)	Encapsulation Efficiency (%[1])	Loading Efficiency (%[2])
100	95.41 ± 3.42	2.06 ± 0.36
300	94.93 ± 3.43	2.23 ± 1.11
500	81.59 ± 6.59	7.30 ± 2.60
700	82.95 ± 15.45	10.72 ± 0.92
1000	74.01 ± 1.8	16.78 ± 0.77

Notes: %[1], The amount of encapsulated curcumin/total curcumin input when forming pHDL-Cur × 100%; %[2], The weight of encapsulated curcumin/the weight of pHDL-Cur × 100%.

technical parameters of microfluidics used for pHDL were applied (5-1-5 mL/min flow rate in external-middle-external channels with 0.2 mg/mL peptides), with an optimal encapsulation efficiency of 94.73 ± 3.43% and loading efficiency of 2.23 ± 1.11% obtained when 300 μg/mL curcumin was loaded (Table 1). Unlike pHDL-Cur, the construction of pHDL-TanIIA required more optimization steps. By initially adjusting flow rates from 2.5-1-2.5 mL/min to 5-1-5 mL/min, then to 10-1-10 mL/min (external-middle-external) in microfluidic channels (Figure S1A), a better result was gained in 10-1-10 mL/min condition. Then, when maintaining the flow rate at a constant of 10-1-10 mL/min while lowering the peptide concentration from 0.2 mg/mL to 0.1 mg/mL, no difference in the productivity of pHDL-TanIIA was found (Figure S1B). Therefore, 0.1 mg/mL instead of 0.2 mg/mL peptides in the external channels was employed for more economic benefits and comparable encapsulation efficiency of TanIIA (100 μg/mL: 94.29%, 200 μg/mL: 98.46%). In addition, to determine the preferential quantity of TanIIA that could be loaded, 100 to 1000 μg/mL TanIIA was sequentially tested. As shown in Table 2, TanIIA at 700 μg/mL appeared to be the best considering both encapsulation efficiency (93.19 ± 1.14%) and loading efficiency (9.09 ± 0.01%) as evaluated by HPLC. Accordingly, we applied the above optimized protocols for pHDL-TanIIA and pHDL-Cur in the following studies.

To elucidate the remodeling of loaded compounds by pHDL, we individually compared the raw forms and pHDL-carried formulations of TanIIA/curcumin, in terms of both morphological alterations and aqueous solubility. Under electron microscopy, both TanIIA and curcumin dispersed as heterogeneous structures in a micro-size scale, and TanIIA presented in a way of more irregularly shaped clumps (Figure 1A), while curcumin exhibited as more prism-like crystals (Figure 1B). In contrast, dramatic alterations were observed when TanIIA or curcumin was entrapped into pHDL. The obtained pHDL-TanIIA nanoformulations had pHDL-like nano-disk architecture but were two-fold larger than those of pHDL, as indicated in the average diameter of 7.62 ± 1.84 nm for pHDL (Figure 1C) and 15.5 ± 2.76 nm for pHDL-TanIIA (Figure 1D). Once incorporated by pHDL, the physical property of TanIIA shifted from insoluble red sediment (Figure 1E) to transparent red solution (Figure 1F and G), demonstrating the efficient encapsulation and improved solubility of TanIIA in pHDL milieu. Similarly, pHDL-Cur inherited the discoidal shape of pHDL with 12.74 ± 2.54 nm in diameter as observed by TEM (Figure 1H). When loaded into pHDL, the indissoluble curcumin shown as yellow particles in suspension (Figure 1I) turned into clear yellow solutions (Figure 1J and K), confirming the capacity of pHDL as nano-carriers for hydrophobic components.

Table 2 Encapsulation and Loading Efficiency of TanIIA into pHDL

Concentration of TanIIA (μg/mL)	Encapsulation Efficiency (%[1])	Loading Efficiency (%[2])
50	98.40	0.10
100	96.34	0.74
400	88.07	4.36
700	93.19 ± 1.14	9.09 ± 0.01
1000	78.57	8.23
1500	49.76	9.25

Notes: %[1], The amount of encapsulated TanIIA/total TanIIA input when forming pHDL-TanIIA × 100%; %[2], The weight of encapsulated TanIIA/the weight of pHDL-TanIIA × 100%.

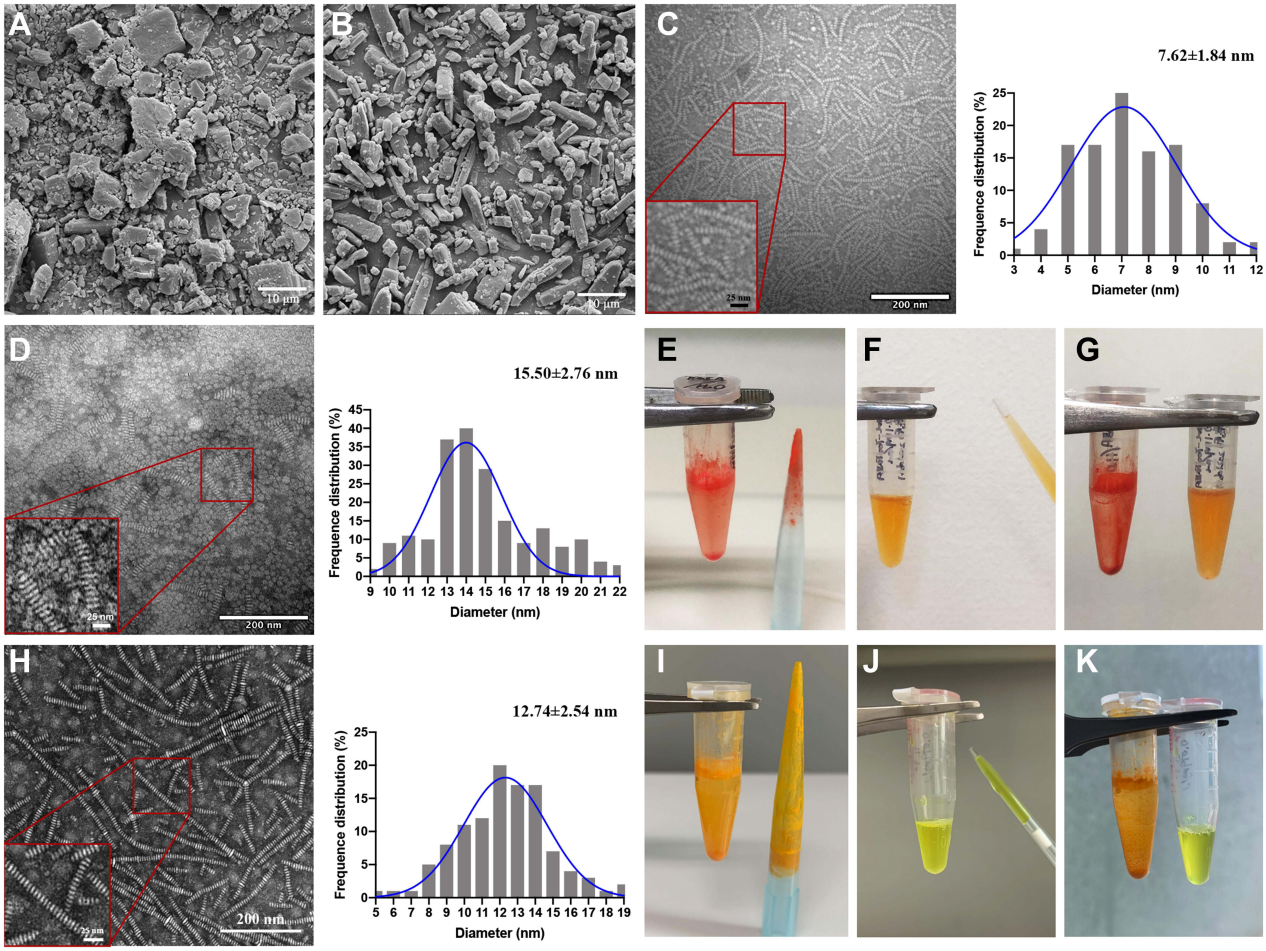

Figure 1 Characterization of pHDL-TanIIA and pHDL-Cur. (**A** and **B**), SEM visualizations of morphological features of TanIIA (**A**) and curcumin (**B**). (**C**), characterizations of pHDL nanoparticles without loaded drugs by TEM (left panel) and the corresponding examination of size distribution (right panel). (**D**–**G**), characterizations of pHDL-TanIIA by TEM (**D**, left panel), the corresponding analysis of size distribution (**D**, right panel), the appearance of free TanIIA in ddH_2O (**E**), pHDL-TanIIA in ddH_2O (**F**), and the comparison of free TanIIA (**G**, left panel) with pHDL-TanIIA in ddH_2O (**G**, right panel). (**H**–**K**), characterizations of pHDL-Cur by TEM (**H**, left panel), the corresponding measurement of size distribution (**H**, right panel), the appearance of free curcumin in ddH_2O (**I**), pHDL-Cur in ddH_2O (**J**), and the comparison of free curcumin (**K**, left panel) with pHDL-Cur in ddH_2O (**K**, right panel).

Drug Localization in pHDL

Since DMPC phospholipid bilayer is formed spontaneously by polar head groups exposed to water and hydrophobic tails buried in interior of layer, the discoidal structure of pHDL is therefore modelled with one side of DMPC tail surrounded by the hydrophobic face of amphipathic peptides, while the polar side-chain and hydrophilic face of peptides exposed to the aqueous milieu to acquire water solubility.[21] Taking advantages of intrinsic UV–Vis absorbance and fluorescence spectrum of curcumin, we explored the location of hydrophobic curcumin in pHDL particles. Being hydrophobic, curcumin could either present in the hydrophobic milieu of the fatty acyl chains in lipid bilayer or interact with the hydrophobic face of peptides.

To address the first possibility, the association of curcumin with phospholipid was determined by comparing insoluble curcumin suspension, ethanol solution of curcumin and pHDL-Cur according to the absorbance and fluorescence spectrum of curcumin. Compared to curcumin suspension in ddH_2O, where no absorbance was detected (Figure 2Ai), curcumin dissolved in ethanol resulted in a broad absorbance spectrum with a single major peak at 427 nm (Figure 2Aii). When entrapped in pHDL, the spectrum of pHDL-Cur in ddH_2O was blue shifted to 420 nm from that of free curcumin in ethanol (Figure 2Aiii), indicating solubilization of curcumin in pHDL milieu and the presence of curcumin in a relatively nonpolar environment of pHDL carrier. This result was consistent with recordings using fluorescence

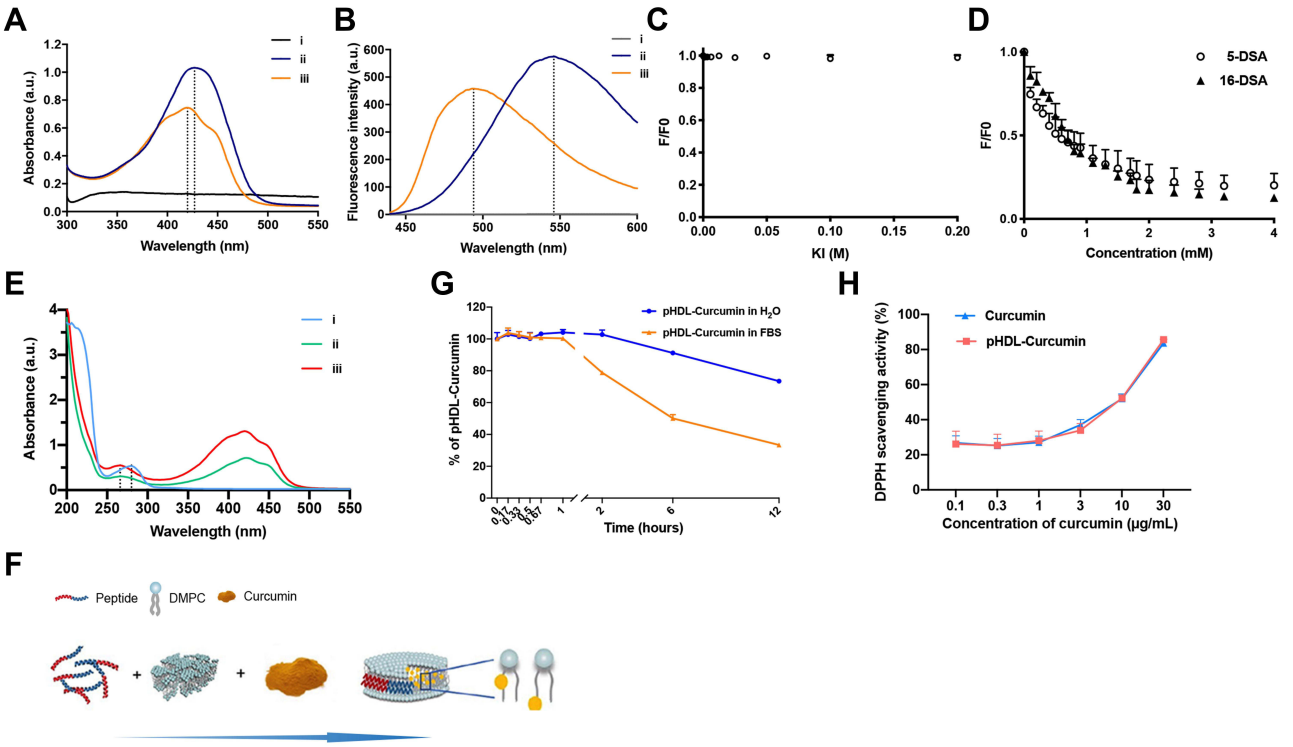

Figure 2 Characterization of curcumin in pHDL-Cur. (**A**), the UV-vis absorbance spectra of free curcumin in ddH_2O (i), in ethanol (ii), and pHDL-Cur in ddH_2O (iii). (**B**), the fluorescence emission spectra of free curcumin in ddH_2O (i), in ethanol (iii), and pHDL-Cur in ddH_2O (iii), with excitation at 420 nm. (**C** and **D**), quenching analysis of curcumin in pHDL-Cur by increasing concentrations of KI in ddH_2O (**C**) or DOXYL-stearic acid (5-DSA or 16-DSA) in DMSO (**D**), with fluorescence emission intensity recorded at 494 nm (excitation at 420 nm). Data are plotted as F/F_0 versus quencher concentration. (**E**), the UV-vis absorbance spectra of pHDL in ddH_2O (i), 300 μg/mL pHDL-Cur in ddH_2O (ii), and 500 μg/mL pHDL-Cur in ddH_2O (iii). (**F**), Schematic depiction of pHDL-Cur construction. (**G**), stability of pHDL-Cur in ddH_2O and FBS at 37°C over a 12 h incubation period. Data were plotted as % of time 0. (**H**), anti-oxidative activities measured as relative intensity of the maximum absorption of DPPH in the presence of free curcumin and pHDL-Cur at 25°C.

spectrum of different curcumin preparations, which revealed that free curcumin in ddH_2O did not show detectable fluoresce (Figure 2Bi), whereas the excitation of curcumin in ethanol gave rise to an emission peak centered at 546 nm (excitation 420 nm, Figure 2Bii), and the maximal fluorescence for pHDL-Cur was blue shifted to 493 nm (Figure 2Biii). Based on the evidence of a strong blue-shifted spectrum, we speculate that curcumin is deeply located within the lipid bilayer of pHDL. To further verify the location of curcumin within lipid bilayer of pHDL, two types of fluorescence quenchers known as water-soluble (potassium iodide, KI) and lipid-soluble (5-doxyl-stearic acids (5-DSA) and 16-doxyl-stearic acids (16-DSA)) were used to quench the fluorescence emission of curcumin. This set of analyses was designed based on the fact that if curcumin located on the surface of pHDL facing aqueous environment, the fluorescence of curcumin would be quenched by KI; by contrast, when curcumin was carried in deeper hydrophobic region of pHDL, quenching constants using 5-DSA and 16-DSA would be dominant due to the insertion of their doxyl group in hydrophobic tail, with 16-DSA embedded deeper than 5-DSA. As presented in plots of F/F_0 versus quencher concentration for quenching of curcumin fluorescence with augmented KI (Figure 2C) and doxyl-stearic acids (Figure 2D), both doxyl-stearic acids were far more powerful in quenching compared to KI, displaying apparent Stern-Volmer quenching constants of $2.09 \pm 0.11 \times 10^{-3}$ M^{-1} for 16-DSA and relatively lower $1.29 \pm 0.11 \times 10^{-3}$ M^{-1} for 5-DSA (Figure 2D) versus 0.05 ± 0.04 M^{-1} for KI (Figure 2C). Our results are similar to what Elsy et al found in curcumin contained in DMPC liposomes, where the most pronounced quenching effects were observed in non-polar regions buried between the lipid chains.[32] In particular, from comparisons of quenching curves showing that Ksv of 16-DSA is about 1.6-fold higher than that for 5-DSA, we propose that curcumin extends along the full length of acyl-chain and preferably situates in a relatively deeper hydrophobic region of pHDL.

To determine whether curcumin has interactions with the hydrophobic face of peptides, we then analyzed the absorbance spectrum of pHDL and pHDL-Cur at 300 μg/mL and 500 μg/mL, respectively. In general, the absorption

spectra of the aromatic amino acids are the primary determinants for the typical absorbance peak at 280 nm[33] (Figure 2Ei). Upon loading with different dosages of curcumin, the peptide yielded a 14 nm blue shift of absorption, indicating a potential conformation change of peptides due to the interaction with curcumin (Figure 2Eii and Eiii). When raising pHDL-Cur from 300 μg/mL to 500 μg/mL, an increased absorption at the peak of 266 nm (modified peptides) and 420 nm (pHDL-Cur) was detected (Figure 2Eii and Eiii), confirming the interaction of loaded curcumin with the hydrophobic side of amphipathic peptides in a dose-dependent manner. Collectively, we provide evidence that the entrapped curcumin situates in the deeper hydrophobic region of DMPC, where it contacts with the hydrophobic face of amphipathic peptide (Figure 2F).

In addition to improved physicochemical properties, the perseverance of anti-oxidative bioactivities of curcumin in pHDL was further evaluated. Prior to measuring the anti-oxidative functions, we first determined the stability of pHDL-Cur in both H_2O and FBS. As shown in Figure 2G, the pHDL-Cur maintained stability in the initial 1 h of experiments in both H_2O and FBS and then started to lose its integrity in FBS at 2 h time point while kept intact in H_2O. At the end of a 12 h incubation, more than 70% pHDL-Cur could be detected in H_2O, whereas only 30% pHDL-Cur were found stable in FBS. Consistently, a similar stability pattern was captured in the same settings for pHDL-TanIIA (Figure S2A), showing a desired stability within the first 1 h, which was reduced in FBS from 2 h, and remained about 50% at the end of 12 h compared to 80% in H_2O. Based on this finding, the anti-oxidative potential of pHDL-Cur was carried out by a design of a cell-free experiment of 30 min incubation. As shown in Figure 2H, when enhancing non-loaded curcumin from 0.1 μg/mL to 30 μg/mL, a 4-fold increase of anti-oxidative potential of pHDL-Cur was detected by measuring DPPH scavenging rate, which was identical to the pattern observed in the condition of free curcumin, suggesting that though curcumin has a direct contact with elements of pHDL, its fundamental bioactivity maintained unaltered.

Ex vivo Targeting and in vivo Distribution of Drugs Carried by pHDL

Before moving to the evaluation of major biological capacities of drug-loaded pHDL, we performed the cytotoxicity tests for both pHDL-Cur and pHDL-TanIIA using HEK-293T (kidney, Figure S3A), A549 (lung, Figure S3B), HepG2 (liver, Figure S3C), and HUVEC (endothelium, Figure S3D) cells (also see Supplementary Materials and Methods). A similar cytotoxicity profile was observed in pHDL-Cur- and pHDL-TanIIA-treated conditions (Figure S3), which was also concordant with the cytotoxicity pattern of pHDL without drug loading,[21] suggesting a conservation of cellular responses of pHDL when loaded with drugs. Then, with the assistance of intrinsic fluorescence properties of curcumin, the in vivo circulating profile, tissue distribution and plaque-targeting of pHDL-Cur were decided. In the case of curcumin oral administration (Figure 3A, grey), the peak fluorescence was detected at 1 h with a rapid clearance within 2 h post-administration, and a practically non-detectable signal was found at 8 h time point, demonstrating a fast elimination of curcumin. Unlike the dynamic circulating profile of pHDL, which had a maximum serum pHDL level around 8 h after *ip* injection in *ApoE*$^{-/-}$ mouse model,[21] the burst of curcumin fluorescence was shown at 30 mins after *ip* exposure of

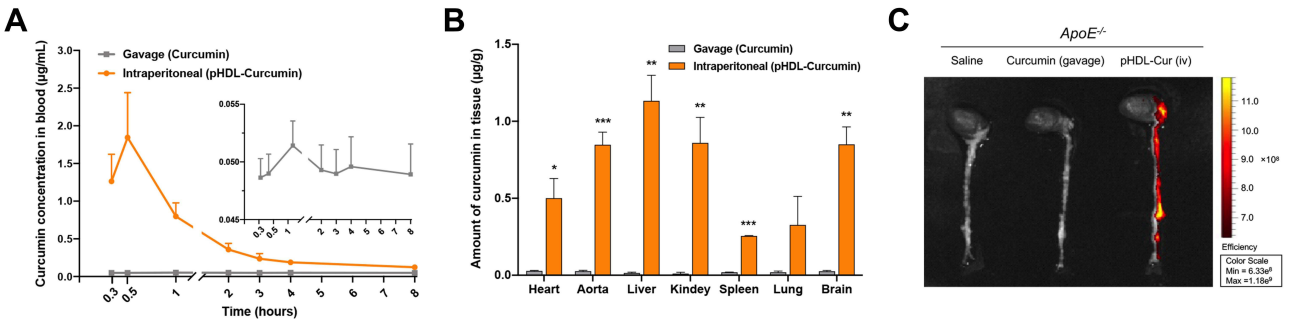

Figure 3 Distribution of pHDL-Cur in blood and tissues of *ApoE* deficient mice. (**A**), dynamic profile of curcumin in blood of *ApoE* deficient mice of 9 months measured at T=0, 0.3, 0.5, 1, 2, 3, 4, and 8 h post *ip* injection of pHDL-Cur or orally administration of free curcumin. (**B**), tissue distribution of curcumin measured at T=0.5 h post pHDL-Cur treatment by *ip* injection or free curcumin by gavage. (**C**), fluorescence image of curcumin in isolated heart and aorta of *ApoE* deficient mice treated with either saline by *iv* injection, or curcumin by gavage or pHDL-Cur by *iv* injection. Indicators of fluorescence intensity are shown on the right. Data are average of at least 3 animals and expressed as mean±SEM. *P<0.05; **P<0.01; and ***P<0.005 vs corresponding curcumin by gavage.

pHDL-Cur in *ApoE* deficient mice, with 5.4% remained in serum 8 h after injection (Figure 3A, orange). This pattern is consistent with previous reports, showing a higher level of curcumin formulated in nanoparticles with an initial peak followed by a moderate decrease in plasma level over time.[34] When compared with free curcumin administered by gavage, the maximum serum signal of curcumin in pHDL-Cur was 36.4-fold stronger, indicating an improved bioavailability of curcumin carried by pHDL.

Considering that the biological activity of curcumin is largely dependent on the actual uptake of curcumin into targeted tissues, we then assessed the distribution of curcumin using organs of $ApoE^{-/-}$ mice treated with either free curcumin by gavage or pHDL-Cur. The fluorescent intensities in each organ were analyzed as shown in Figure 3B. Curcumin, which was administered orally, exhibited low levels of fluorescent signals in collected tissues, including the heart, aorta, liver, kidney, spleen, lung, and brain (grey). However, when entrapped by pHDL, a general increase in curcumin fluorescence was obtained (orange), which is in great agreement with the abundance of curcumin detected in the serum of *ApoE* deficient mice. In accordance with previous studies showing that liver and kidney are typical organs of the homing sites for nanoparticles owing to the small size, the highest fluorescence intensity of curcumin was observed in liver, followed by kidney when mice were treated with pHDL-Cur. Intriguingly, a comparable level of renal curcumin was detected in the aorta in pHDL-Cur-exposed group ($p = 0.0006$), which was 28.3-fold of free curcumin, strongly suggesting that pHDL is functioning as an efficient vehicle delivering curcumin to the plaque lesions of AS models. It is noteworthy that the brain, which expresses a high level of SR-B1 as HDL receptor, also showed augmented curcumin signals, providing clues that pHDL is potentially beneficial to deliver curcumin across the blood–brain barrier. The favorable distribution of encapsulated drugs by pHDL was additionally confirmed by HPLC using pHDL-TanIIA-treated $AopE^{-/-}$ mice (Figure S2B). Following that, we proceeded to evaluate the preferential and specific targeting of pHDL to atherosclerotic lesion area in $ApoE^{-/-}$ mice, as compared to C57BL/6J control animals. To achieve this goal, we first proved that pHDL itself was capable of plaque-targeting by using FITC-labelled pHDL to facilitate fluorescence imaging in situ or with excised heart and aorta. The imaging of excised aortas revealed the accumulation of FITC-pHDL located along the aorta and the aortic root, the regions where atherosclerotic lesions are typically present in this disease model (Figure S4). To further investigate the efficiency of pHDL as a drug carrier, we then desired to verify the recruitment of drugs encapsulated by pHDL to the site of atherosclerotic plaque using ex vivo optical fluorescence imaging. As demonstrated in Figure 3C, only a negligible strength of fluorescence was detected in the aorta and heart of animals from saline or curcumin group. In contrast, a strong fluorescence signal can be clearly visualized along the aorta and aortic root of pHDL-Cur-challenged animals, confirming the plaque-targeted delivery efficiency of pHDL in the model of AS. Collectively, our results showed an improved bioavailability and association of curcumin with atherosclerotic lesions by pHDL-based formulations.

In vivo Anti-Atherogenic Efficacies in $ApoE^{-/-}$ Mice

To test whether enhanced bioavailability and recruitment of encapsulated drugs by pHDL give rise to more effective protection against AS, we treated $ApoE^{-/-}$ mice on HFD with drugs encapsulated by pHDL and shortened the therapeutic intervention to 6 weeks after 8-week HFD priming, instead of 12 weeks after 8-week HFD priming in previous studies.[21] A group of C57BL/6J mice on a normal diet was included as baseline control, as shown in the schematic illustration (Figure 4A).

Aiming to simultaneously control both lipid metabolism and associated inflammation, TanIIA that has been recognized as an anti-inflammatory candidate in protections against cardiovascular disorders is accordingly selected, based on the fact that pHDL is potent in the correction of dyslipidemia. As shown in Figure 4B–D, plasma TG, TC, and LDL-C increased significantly in the $ApoE^{-/-}$ mice after continuous 8-week HFD priming and 6-week HFD plus pHDL-TanIIA treatment (14-week HFD in total), as compared with the corresponding levels in C57BL/6J mice. As expected, pHDL-TanIIA exhibited an improved lipid profile in comparison with pHDL or TanIIA alone, showing substantially reduced TG level by 45.44% (p=0.00005, pHDL: −30.05%, TanIIA: −24.73%), significantly lowered TC by 25.75% (p=0.022, pHDL: −18.85%, TanIIA: −14.4%), and slightly decreased LDL-C by 16.02% (pHDL: −14%, TanIIA: −7.45%) in comparison with $ApoE^{-/-}$ mice treated with saline control. To further investigate the role of pHDL-TanIIA in atherosclerotic plaque formation, the histological assessment of atherosclerotic burden in the aortic sinus area was performed,

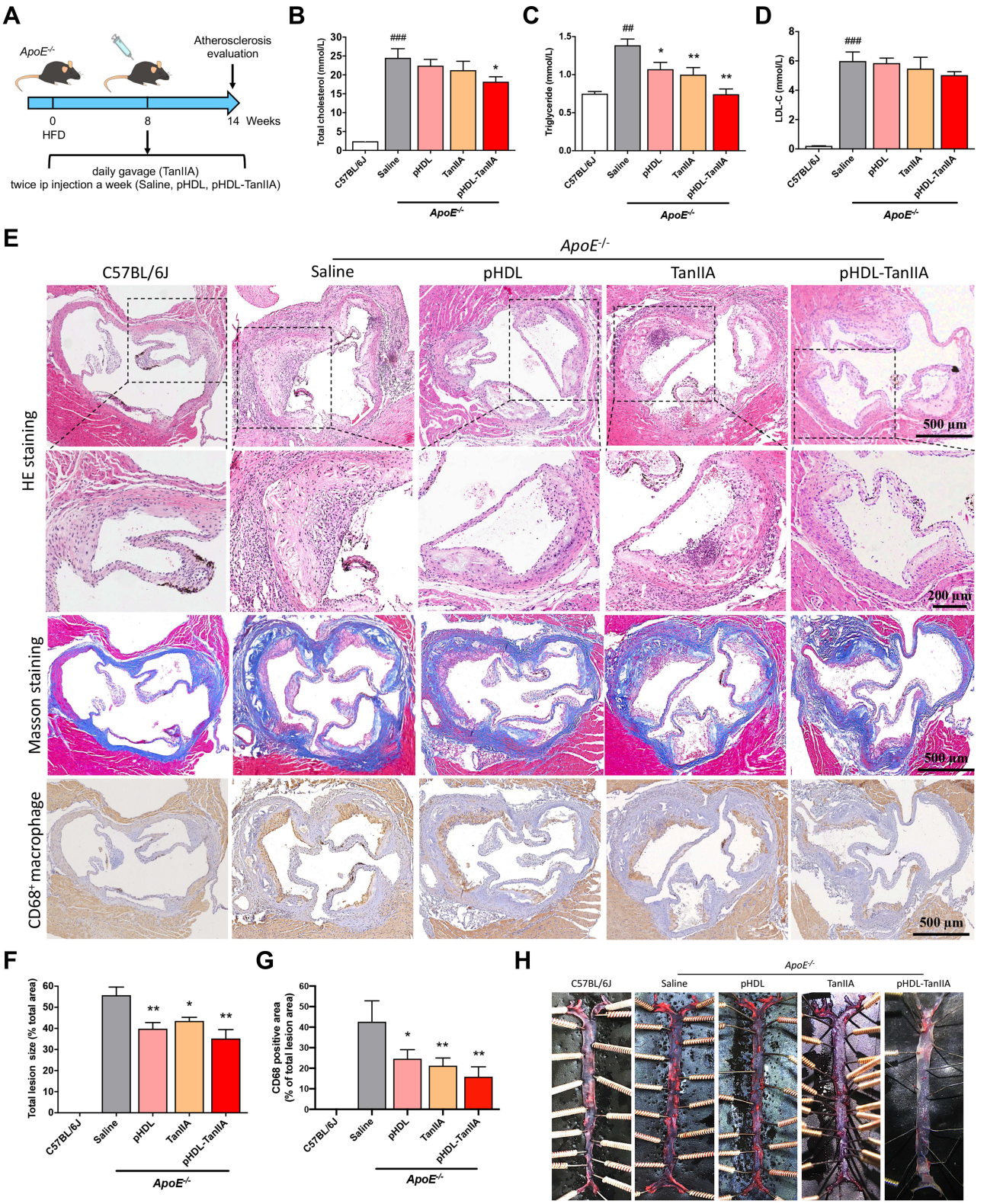

Figure 4 Anti-AS efficacy of pHDL-TanIIA in *ApoE* deficient mice. (**A**), experimental design for the study evaluating anti-AS efficacy of pHDL-TanIIA with *ApoE* deficient mice on HFD. (**B**–**D**), biochemistry analysis of total cholesterol (**B**), total triglyceride (**C**), and LDL-C (**D**) in *ApoE* deficient mice challenged with either saline, or pHDL, or TanIIA by gavage, or pHDL-TanIIA, compared to C57BL/6J wild-type animals as basal control. (**E**), cross sections of aortic roots for the assessment of atherosclerotic lesions stained with HE, Masson Trichrome, and immunohistochemical staining for CD68. For HE staining, corresponding magnified areas of the boxed regions are marked as indicated, scale bar=500μm. (**F** and **G**), quantification of atherosclerotic lesions for HE staining (**F**) and $CD68^+$ macrophages (**G**). (**H**), representative images of en face Oil-red O staining for the overall plaque formation in aorta trunk (thoracic and abdominal). (**B, C, D, F** and **G**), data are plotted by averaging of 6–7 mice per group and presented as mean±SEM. $^{\#\#}P<0.01$; and $^{\#\#\#}P<0.005$ vs C57BL/6J control. $^{*}P<0.05$; and $^{**}P<0.01$ vs $ApoE^{-/-}$ exposed to saline.

where plaque formation occurred more rapidly and consistently than abdominal aorta. As presented in Figure 4E, following a 14-week HFD, atherosclerotic lesion that is predominantly composed of foam cells and macrophage-like cells was observed in the aortic root of *ApoE*$^{-/-}$ mice. Compared to model mice without therapeutic interventions, animals treated with pHDL-TanIIA revealed a significant reduction in lesion areas, as shown by HE staining, the Masson Trichrome staining for collagen, and the immunostaining of macrophage-specific marker CD68 (Figure 4E). Further assessment of plaque areas revealed that pHDL-TanIIA curtailed 36.86% plaque regions (p=0.0001), while a 28.5% decline and a 21.96% decrease were found in pHDL- and TanIIA-treated group, respectively (Figure 4F). In addition, quantifications of macrophage content within lesions demonstrated that there was a 62.7% decrease in the areas of CD68^{+} macrophage when treated with pHDL-TanIIA (p=0.0006), possibly reflecting a synergistic effect benefited from that of pHDL (−42.3%) (p=0.01) and TanIIA (−50.3%) (p=0.0019) (Figure 4G). The favorable responses of pHDL-TanIIA in regulating dyslipidemia and inflammation could be successfully translated to athero-protection in *ApoE*$^{-/-}$ mice, as the overall plaque lesions across the whole aorta trunk were dramatically lessened in contrast to those treated with either pHDL or TanIIA (Figure 4H). Altogether, data from in vivo experiments proved in therapeutic potentials that pHDL-assisted TanIIA delivery is more effective in ameliorating the progress of AS.

Favorable Protective Effects on Liver and Kidney in *ApoE*$^{-/-}$ Mice

During the whole period of experiments, we did not observe obvious side effects such as weight loss and local irritation in *ApoE*$^{-/-}$ mice. At the time of sacrifice, no signs of necrosis or hyperplasia were detected in organs including heart, liver, kidney, spleen, lung, and brain by macroscopic examinations. Considering that pHDL encapsulating components of natural plants were mainly distributed in the liver and kidney of *ApoE*$^{-/-}$ mice, we next investigated the hepatic and renal biocompatibility of pHDL-TanIIA, respectively. The biochemical parameters of blood serum were determined, incorporating TanIIA potentiated the improvement of ALT (p=0.002) (Figure 5A), AST (p=0.000018) (Figure 5B), globulin

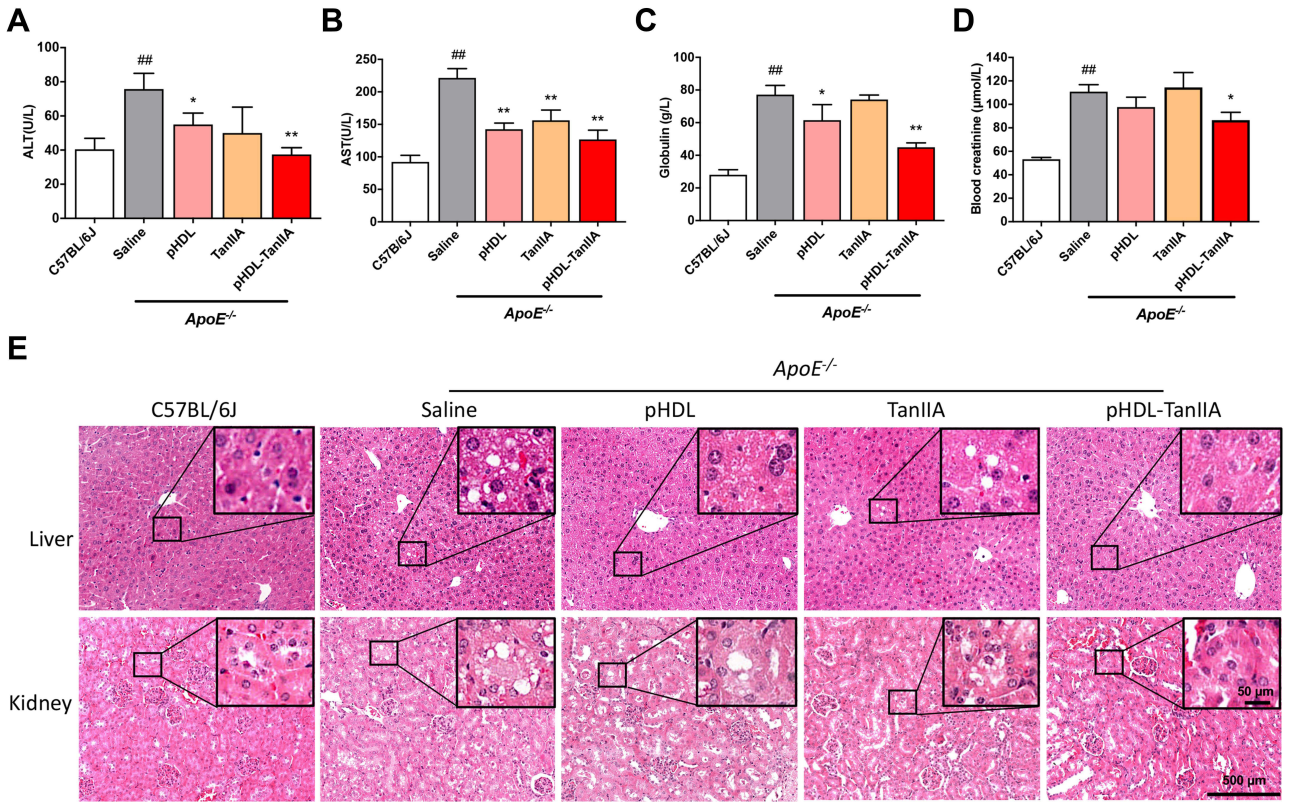

Figure 5 Protective effect of pHDL-TanIIA on liver and kidney in *ApoE* deficient mice. (**A**–**D**), serum levels of ALT (**A**), AST (**B**), globulin (**C**) and creatinine (**D**). (**E**), representative images of HE staining of liver (upper panels) and kidney (lower panels) sections of experimental mice. Inlets are the corresponding magnified areas of the boxed regions as indicated, scale bar=500μm. ##P<0.01 vs C57BL/6J control mice. *P<0.05; and **P<0.01 vs *ApoE*$^{-/-}$ AS model treated with saline.

(p=0.003) (Figure 5C), and blood creatinine (p=0.038) (Figure 5D) established by pHDL. Further histological examinations of the liver revealed microvesicular steatosis characterized by the presence of numerous small vesicles of fat in hepatocytes and sporadically accompanied by fat-engorged hepatocytes in HFD-fed *ApoE*$^{-/-}$ mice (Figure 5E, upper panels). Similarly, numerous cytoplasmic vacuoles could be observed in renal tubule cells of HFD-fed *ApoE*$^{-/-}$ mice when compared to that of C57BL/6J mice (Figure 5E, lower panels). By treating animals with pHDL-TanIIA, the fatty degeneration in both liver and kidney was extensively ameliorated, which was more prominent compared to mice challenged with either pHDL or TanIIA for 6 weeks (Figure 5). Taken together, our data clearly show in vivo evidence that pHDL-TanIIA synergistically counteracts AS-associated consequences.

Conclusions

Herein, we show that pHDL carrying either TanIIA (pHDL-TanIIA) or curcumin (pHDL-Cur) can be successfully constructed by simply manipulating ratios of mixture and speeds during microfluidics. Both TanIIA and curcumin entrapped into pHDL acquire discoidal morphology as that of native HDL particles and gain a favorable feature of water solubility. Taking advantages of curcumin, which has intrinsic absorbance and fluorescence properties, we confirm that lipophilic curcumin is encapsulated inside the phospholipid core of pHDL nanodisks and potentially interacts with the hydrophobic face of peptides. More importantly, pHDL-Cur is stable in physiological conditions and possesses the same antioxidant activity as free curcumin. In addition, we reveal that curcumin can be typically recruited to the site of atherosclerotic plaque with the assistance of pHDL ex vivo, confirming the targeted-delivery capacities by pHDL. With respect to anti-AS effects, the incorporation of TanIIA in pHDL exhibits greater benefits against the progress of AS plaque than pHDL or TanIIA alone in *ApoE*-deficient atherosclerotic mouse model, verifying and extending the potential of pHDL-based therapies. Overall, our work supports the targeted-drug delivery and anti-AS capacity of pHDL, which provides insights into pHDL-derived approaches as prospective therapeutic candidates for AS. Currently, since several ongoing therapeutics associated with HDL have been intensively evaluated in clinical trials, the implementation involving pHDL-based therapies, which provide comparable efficacy with a more economical procedure compared to conventional HDL nanoparticles, will potentially facilitate the clinical translation of HDL-based therapies, and extend the application scenarios of HDL-related strategies as a drug carrier for targeted delivery of anti-AS drugs. More importantly, the presented approach allows the incorporation and utilization of a diversity of bioactive chemicals isolated from natural plants which are currently underutilized due to features like low bioavailability.

Abbrevations

pHDL, peptide-based high-density lipoprotein; AS, atherosclerosis; Cur, curcumin; TanIIA, tanshinone IIA; HPLC, high-performance liquid chromatography; CVD, cardiovascular disease; WHO, World Health Organization; IL-1Ra, interleukin-1 receptor antagonist; IL-6Rb, blocker of IL-6 receptor; HDL, high-density lipoprotein; RCT, reverse cholesterol transport; ApoA-1, apolipoprotein A-1; ABCA1, ATP-binding cassette transporter A1; ABCG1, ATP-binding cassette transporter G1; SR-B1, scavenger receptor B1; SD-UC, sequential density ultracentrifugation; FPLC, fast protein liquid chromatography; FITC, fluorescein isothiocyanate; KI, potassium iodide; CD, chow diet; HFD, high fat diet; ip, intraperitoneal; iv, intravenous; TC, total cholesterol; TG, triglyceride; LDL-C, low-density lipoprotein cholesterol; ALT, alanine aminotransferase; AST, aspartate aminotransferase; ddH_2O, double distilled water; 5-DSA, 5-doxyl-stearic acids; 16-DSA, 16-doxyl-stearic acids.

Acknowledgment

The authors thank Prof. Zhenji Li, The World Federation of Chinese Medicine Societies, for his support and valuable input. Present address for Ziyun Li, The Third School of Clinical Medicine, Nanjing University of Chinese Medicine, Nanjing, China.

Author Contributions

All authors made substantial contributions to the design and conception of the study and acquisition, analysis and interpretation of data and took part in either drafting or revising the manuscript. All authors gave final approval of the

version to be published, have agreed on the journal to which the article has been submitted, and agreed to be accountable for all aspects of the work in ensuring that questions related to the accuracy or integrity of any part of the work are appropriately investigated and resolved.

Funding

This work was supported by the Scientific and Technological Innovation Project, China Academy of Chinese Medical Sciences (CI2021A00112), Beijing Traditional Chinese Medicine Technology Development Foundation (JJ-2020-85), and the Fundamental Research Funds for the Central Public Welfare Research Institutes (YZ-202110).

Disclosure

Author Wei Xiao is employed by Jiangsu Kanion Pharmaceutical Co.Ltd. The remaining authors declare that the research was conducted in the absence of any commercial or financial relationships that could be constructed as a potential conflict of interest.

References

1. Libby P, Buring JE, Badimon L, et al. Atherosclerosis. *Nat Rev Dis Primers*. 2019;5:56. doi:10.1038/s41572-019-0106-z
2. Ross R, Epstein FH. Atherosclerosis – an inflammatory disease. *N Engl J Med*. 1999;340:115–126. doi:10.1056/NEJM199901143400207
3. Lusis AJ. Atherosclerosis. *Nature*. 2000;407:233–241. doi:10.1038/35025203
4. Virmani R, Kolodgie FD, Burke AP, et al. Atherosclerotic plaque progression and vulnerability to rupture, angiogenesis as a source of intraplaque hemorrhage. *Arterioscler Thromb Vasc Biol*. 2005;25:2054–2061. doi:10.1161/01.ATV.0000178991.71605.18
5. Macedo AF, Taylor FC, Casas JP, Adler A, Prieto-Merino D, Ebrahim S. Unintended effects of statins from observational studies in the general population, systematic review and meta-analysis. *BMC Med*. 2014;12:51. doi:10.1186/1741-7015-12-51
6. Herder C, Donath MY. Interleukin-1 receptor antagonist, friend or foe to the heart? *Lancet Diabetes Endocrinol*. 2015;3:228–229. doi:10.1016/S2213-8587(15)00035-2
7. Hartman J, Frishman WH. Inflammation and atherosclerosis, a review of the role of interleukin-6 in the development of atherosclerosis and the potential for targeted drug therapy. *Cardiol Rev*. 2014;22(3):147–151. doi:10.1097/CRD.0000000000000021
8. Cheng Z, Li M, Dey R, Chen Y. Nanomaterials for cancer therapy, current progress and perspectives. *J Hematol Oncol*. 2021;14:85. doi:10.1186/s13045-021-01096-0
9. Chen J, Zhang X, Millican R, et al. Recent advances in nanomaterials for therapy and diagnosis for atherosclerosis. *Adv Drug Deliv Rev*. 2021;170:142–199. doi:10.1016/j.addr.2021.01.005
10. Sanchez-Gaytan BL, Fay F, Lobatto ME, et al. HDL-mimetic PLGA nanoparticle to target atherosclerosis plaque macrophages. *Bioconjug Chem*. 2015;26(3):443–451. doi:10.1021/bc500517k
11. Kingwell BA, Chapman MJ, Kontush A, Miller NE. HDL-targeted therapies, progress, failures and future. *Nat Rev Drug Discov*. 2014;13:445–464. doi:10.1038/nrd4279
12. Ouimet M, Barrett TJ, Fisher EA. HDL and reverse cholesterol transport. *Circ Res*. 2019;124:1505–1518. doi:10.1161/CIRCRESAHA.119.312617
13. Sorci-Thomas MG, Owen JS, Fulp B, et al. Nascent high density lipoproteins formed by ABCA1 resemble lipid rafts and are structurally organized by three apoA-I monomers. *J Lipid Res*. 2012;53:1890–1909. doi:10.1194/jlr.M026674
14. Li K, Wong DK, Luk FS, Kim RY, Raffai RL. Isolation of plasma lipoproteins as a source of extracellular RNA. *Methods Mol Biol*. 2018;1740:139–153.
15. Plochberger B, Rohrl C, Preiner J, et al. HDL particles incorporate into lipid bilayers - a combined AFM and single molecule fluorescence microscopy study. *Sci Rep*. 2017;7:15886. doi:10.1038/s41598-017-15949-7
16. Benito-Vicente A, Martin C, Blanco-Vaca F, Rotllan N, Rotllan N. (r)HDL in theranostics, how do we apply HDL's biology for precision medicine in atherosclerosis management? *Biomater Sci*. 2021;9:3185–3208. doi:10.1039/D0BM01838D
17. Kuai R, Li D, Chen YE, Moon JJ, Schwendeman A. High-density lipoproteins, nature's multifunctional nanoparticles. *ACS Nano*. 2016;10:3015–3041. doi:10.1021/acsnano.5b07522
18. Kim Y, Fay F, Cormode DP, et al. Single step reconstitution of multifunctional high-density lipoprotein-derived nanomaterials using microfluidics. *ACS Nano*. 2013;7:9975–9983. doi:10.1021/nn4039063
19. Binderup T, Duivenvoorden R, Fay F, et al. Imaging-assisted nanoimmunotherapy for atherosclerosis in multiple species. *Sci Transl Med*. 2019;11. doi:10.1126/scitranslmed.aaw7736
20. Schwendeman A, Sviridov DO, Yuan W, et al. The effect of phospholipid composition of reconstituted HDL on its cholesterol efflux and anti-inflammatory properties. *J Lipid Res*. 2015;56:1727–1737. doi:10.1194/jlr.M060285
21. Xu RD, Li SZ, Shi MF, et al. Peptide-based high-density lipoprotein promotes adipose tissue browning and restrains development of atherosclerosis and type 2 diabetes. *Nano Today*. 2021;36:101054. doi:10.1016/j.nantod.2020.101054
22. Jian X, Liu Y, Zhao Z, Zhao L, Wang D, Liu Q. The role of traditional Chinese medicine in the treatment of atherosclerosis through the regulation of macrophage activity. *Biomed Pharmacother*. 2019;118:109375. doi:10.1016/j.biopha.2019.109375
23. Zhang S, Zou J, Li P, Zheng X, Feng D. Curcumin protects against atherosclerosis in apolipoprotein E-knockout mice by inhibiting toll-like receptor 4 expression. *J Agric Food Chem*. 2018;66:449–456. doi:10.1021/acs.jafc.7b04260
24. Chen Z, Gao X, Jiao Y, et al. Tanshinone IIA exerts anti-inflammatory and immune-regulating effects on vulnerable atherosclerotic plaque partially via the TLR4/MyD88/NF-kappaB signal pathway. *Front Pharmacol*. 2019;10:850. doi:10.3389/fphar.2019.00850

25. Cao J, Ye B, Lin L, et al. Curcumin alleviates oxLDL induced MMP-9 and EMMPRIN expression through the inhibition of NF-kappaB and MAPK pathways in macrophages. *Front Pharmacol*. 2017;8:62. doi:10.3389/fphar.2017.00062
26. Lakowicz J. *Principles of Fluorescence Spectroscopy*. 2nd ed. New York: Kluwer Academic/Plenum; 1999.
27. Eftink MR, Ghiron CA. Exposure of tryptophanyl residues in proteins. Quantitative determination by fluorescence quenching studies. *Biochemistry*. 1976;15:672–680. doi:10.1021/bi00648a035
28. Blois MS. Antioxidant determinations by the use of a stable free radical. *Nature*. 1958;181:1199–1200. doi:10.1038/1811199a0
29. Flores AM, Ye J, Jarr KU, Hosseini-Nassab N, Smith BR, Leeper NJ. Nanoparticle therapy for vascular diseases. *Arterioscler Thromb Vasc Biol*. 2019;39:635–646. doi:10.1161/ATVBAHA.118.311569
30. Guo R, Li L, Su J, et al. Pharmacological activity and mechanism of tanshinone IIA in related diseases. *Drug Des Devel Ther*. 2020;14:4735–4748. doi:10.2147/DDDT.S266911
31. Pourbagher-Shahri AM, Farkhondeh T, Ashrafizadeh M, Talebi M, Samargahndian S. Curcumin and cardiovascular diseases. Focus on cellular targets and cascades. *Biomed Pharmacother*. 2021;136:111214. doi:10.1016/j.biopha.2020.111214
32. El Khoury E, Patra D. Length of hydrocarbon chain influences location of curcumin in liposomes, curcumin as a molecular probe to study ethanol induced interdigitation of liposomes. *J Photochem Photobiol B*. 2016;158:49–54. doi:10.1016/j.jphotobiol.2016.02.022
33. Antosiewicz JM, Shugar D. UV-Vis spectroscopy of tyrosine side-groups in studies of protein structure. Part 2, selected applications. *Biophys Rev*. 2016;8:163–177. doi:10.1007/s12551-016-0197-7
34. Brotons-Canto A, Gonzalez-Navarro CJ, Gil AG, Asin-Prieto E, Saiz MJ, Llabres JM. Zein nanoparticles improve the oral bioavailability of curcumin in Wistar rats. *Pharmaceutics*. 2021;13(3):361. doi:10.3390/pharmaceutics13030361